



Repositorio Institucional de la Universidad Autónoma de Madrid
<https://repositorio.uam.es>

Esta es la **versión de autor** del artículo publicado en:
This is an **author produced version** of a paper published in:

Chemical Communications 57.95 (2021): 12712-12724

DOI: <https://doi.org/10.1039/d1cc04968b>

Copyright: © 2021 The Royal Society of Chemistry

El acceso a la versión del editor puede requerir la suscripción del recurso
Access to the published version may require subscription

Chiral Nanotubes Self-Assembled from Discrete Non-Covalent Macrocycles

P. B. Chamorro,^a F. Aparicio^{*a}

Received 00th January 20xx,
Accepted 00th January 20xx

DOI: 10.1039/x0xx00000x

www.rsc.org/

Many strategies have been used to construct supramolecular hollow tubes, including helical folding of oligomers, bundling of rod-like structures, rolling-up of sheets and stacking of covalent cycles. On the other hand, the interest in controlling chirality at the supramolecular level continues attracting much interest because of its implication in future applications of porous systems. This review article covers the main examples in the literature that use simple molecular structures as chiral units for their precise assembly into discrete non-covalent cyclic structures able to form chiral supramolecular tubular systems.

Introduction

Inspired by tubular organizations found in Nature, many researchers have been interested in creating nano-sized tubular systems due to their potential applications¹⁻⁴ as materials for efficient selective encapsulation, transport, or catalysis.

In particular, the formation of supramolecular nanotubes has attracted enormous attention.⁵⁻⁹ Even though, covalent nanotubes result more robust than supramolecular ones, the advantages that offers the latest makes them promising systems for future applications. Some of these advantages comprise a simpler chemical synthesis and adaptability through

the design of the monomer structure, and advantages derived from the supramolecular process itself like self-recognition and self-organization, among others.

There are several methodologies for the construction of non-covalent nanotubes making use of weak and reversible supramolecular interactions, such as hydrogen bonds, hydrophobic forces, π - π stacking, and metal-ligand coordination. Examples of some of these strategies are the helical folding of oligomers, bundling of rod-like structures, rolling-up of sheets and stacking of covalent or non-covalent cyclic units. Some review articles have been published covering most of these examples.^{6, 8, 9} In this review, we will focus on recent progress in the formation of nanotubes from the self-assembly of discrete non-covalent macrocycles with particular attention to those possessing chiral information (Fig. 1.).

^a Nanostructured Molecular Systems and Materials (MSMn) group, Departamento de Química Orgánica, Facultad de Ciencias, Universidad Autónoma de Madrid, 28049 Madrid, Spain. E-mail: fatima.aparicio@uam.es



Paula Blue Chamorro (Madrid, 1994) obtained her Chemistry degree in 2016 from the Universidad de Alcalá de Henares. Next year, she graduated in Organic Chemistry Master's degree from the Universidad Autónoma de Madrid, where she realized her master's dissertation in the group of Prof. David González Rodríguez (MSMn). Since February 2018, she is carrying out her doctoral thesis

under the supervision of Prof. David González Rodríguez and Dr. Fátima Aparicio. She is working in the creation of novel materials from the self-assembly of smart molecules with amphiphilic nature.



Dr. Fátima Aparicio obtained her PhD degree in 2014 working with Prof. Luis Sánchez on Chirality in Supramolecular Polymers at Universidad Complutense de Madrid (Spain). She carried out a predoctoral stay of 6 months in Prof. Carsten Schmuck's research group (Germany) and a 2-years postdoctoral stay in Prof. Marc Sallé's research group (France). In 2016, she joined Prof. David

González Rodríguez's research group at the Universidad Autónoma de Madrid funded by two Marie Skłodowska-Curie Fellowships: Cofund (2017-2019) and Individual Fellowship (2019-2021). She has recently been awarded with her first project as main researcher funded from the Spanish MICINN (2021-2024).

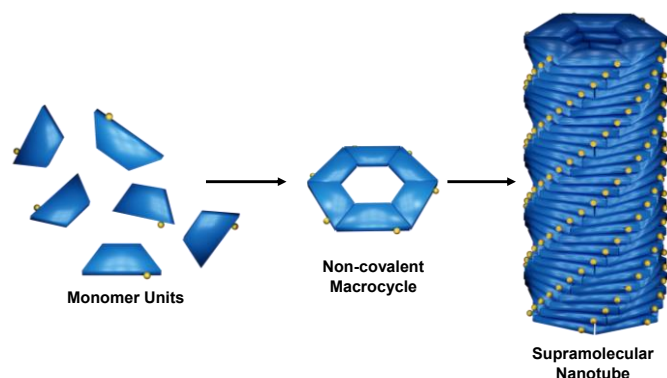


Fig 1. Self-assembly of chiral monomer units through non-covalent forces into a cyclic structure and a supramolecular nanotube. Small yellow balls are included to illustrate chiral motifs in monomer units and to show the formation of a helical nanotube with a preferred handedness.

The function of many biomolecules is governed by the chirality of their components and, consequently, by the final supramolecular chirality embedded in their ensemble. For that reason, simply controlling chirality at the molecular level,^{10–13} that is, in the individual units comprising the cyclic structure that will stack forming the final nanotube, allows controlling the chirality of tubular nanostructures that will determine their potential applications as porous systems.

The use of discrete non-covalent macrocycles as stacking units provides a significant asset, as it is possible to create nanotubes with precise inner and outer diameters through an accurate design of the monomer structure. Even though this could be controlled even more precisely using covalent macrocycles and taking into account that this “preformed” macrocycles do not entail any entropic penalty for ring closure, non-covalent macrocycles offer the advantage of providing well-defined nanotubes from smaller and more synthetically accessible monomer units, that can be prepared with lower efforts and in a more straightforward manner. Thus, key in the molecular design is the preorganization of the system to favour interactions in the pertinent orientation and position. The optimization of chelate cooperativity, that is, the increase in the thermodynamic stability of cyclic structures with respect to linear oligomers, results crucial.^{14–17} In that way, favouring intramolecular association against intermolecular aggregation, will lead to higher chelate effects and higher effective molarities (EM), which is the ratio between intra- and intermolecular binding constants.^{18, 19} Thus, the correct preorganization of the monomer structure will avoid the generation of strain and the loss of conformational degrees of freedom upon cyclization, which will optimize enthalpic and entropic terms of EM, respectively, those favouring ring closure.

Most of the review articles found in the literature cover many different examples of supramolecular tubular structures attending to the construction methodologies we mentioned previously and/or the kind of interactions involved with no particular attention to their chirality.^{9, 20, 21} In this feature article, we will illustrate the main molecular structures, nucleobases, oligophenylenes and metal coordination complexes, used as chiral units for their precise assembly into discrete cyclic structures able to stack on top of each other forming chiral

tubular systems. We hope this review can be of interest for researchers looking for versatile strategies for the construction of chiral supramolecular hollow structures.

Nucleobases

Fused complementary nucleobases. The strategy of using heterocycles based on fused guanine (G) and cytosine (C) nucleobases for the construction of supramolecular macrocycles has been extensively developed by Fenniri’s research group.^{5, 22–28} The self-complementarity between the ADD (A = acceptor, D = donor) H-bonding array of guanine and the DAA array of cytosine, enforces the self-assembly into cyclic structures through H-bonds. Even though this kind of structure had been previously proved to generate cyclic hexameric species by Lehn and co-workers,²⁹ Fenniri’s research group was the pioneer in the demonstration of the stacking of supramolecular macrocycles (rossettes) into nanotubes in water solution.²²

In their first design (Compound **1** in Fig. 2a)²² they also included in the general G-C structure a chiral amino acid capable to form intramolecular ionic H-bonds and provide chirality to the final water-soluble assembly. NOESY (*Nuclear Overhauser Effect Spectroscopy*) ¹H NMR experiments performed in 90% H₂O/D₂O displayed NOE contacts between protons from G and C motifs that were attributed to intermolecular contacts. Moreover, electrospray ionization mass spectrometry (ESI-MS) of dilute aqueous solutions showed the presence of peaks corresponding to non-covalent intermediate species (1-mer to 6-mer) of the final hexameric cycle. The presence of CD (*Circular Dichroism*) activity in aqueous solution and the change in absorption with temperature were ascribed to the helical cooperative stacking of rossettes into nanotubes. DLS (*Dynamic Light Scattering*) experiments provided information about the narrow size distribution (92% in the range 19–69 nm) obtained with an average apparent hydrodynamic radius, *R_h*, of 30.4 nm, considering a columnar stack. And, finally, TEM (*Transmission Electron Microscopy*) measurements confirmed the formation of tubular structures of ~4 nm of outer diameter, in agreement with the expected dimensions (Fig. 2b and c). The combination of the techniques used confirmed the cooperative, hierarchical self-assembly process through H-bonding, stacking interactions, and hydrophobic effects to form helical rosette nanotubes.

Considering this model, the group also reported a similar G-C derivative in which an internally fused pyridine was incorporated between both nucleobases (Compound **2** in Fig. 2a).²⁷ SEM (*Scanning Electron Microscopy*) images of the tricyclic compound **2** in water (pH = 2.8) showed nanotubes that were also characterized by AFM (*Atomic Force Microscopy*) and TEM, obtaining outer diameter values of 4.2 ± 0.2 and 4.4 ± 0.2 nm, respectively (Fig. 2d). Thus, the inner and outer diameters were increased by 0.4 and 0.9 nm, respectively, from the bicyclic to the tricyclic structure. The self-assembly in water solution was investigated by UV-Vis, CD and fluorescence spectroscopies (Fig. 2e and f). The CD signal of the tricyclic compound increased ca. 40 × over 7 days reaching a giant molar

ellipticity, with an unprecedented value reported until that moment. The increased of the temperature or the acidification with trifluoroacetic acid cancelled the CD activity confirming the existence of supramolecular chirality. The appearance of a new narrow and red-shifted band at 388 nm in the UV-Vis spectrum for the tricyclic unit and its growth with time and decrease with the increase of temperature was attributed to a *J*-type arrangement. The growth of this *J*-band was associated to the growth of the CD signal centred at the same wavelength that changed with temperature due to its supramolecular character. Moreover, a subtle hypsochromic effect (ca. 8%) was observed over 7 days whereas a pronounced hyperchromic effect (up to ca. 50%) was recorded upon thermally induced disassembly. These changes suggested a two-step formation of the supramolecular nanotubes: the first step (within minutes) leading to rapid formation of nanotubes and the second (within days) during which compounds adopt a particularly favourable supramolecular arrangement for exciton coupling within the nanotube assembly. The singularly strong CD signal obtained for compound **2** corresponded to the new *J*-band formed because of the stronger electric dipole transitions between adjacent larger molecules in the nanotube structure compared to compound **1**.

The research group has also synthesized more complex G-C motifs that feature two G-C units (called “twin G-C motifs”) and self-organize into hexameric macrocycles through 36 hydrogen bonds, which resulted in substantially more stable self-assembled nanotubes. The presence of chiral features in the structure promotes the hierarchical organization into nanotubes in methanolic and aqueous conditions.^{24, 30} Modifications in the chemical structure or the environment produced different phenomena: a) mirror-image supramolecular chirality due to absolute molecular chirality, (b) solvent-induced supramolecular chirality inversion, (c) structure-dependent supramolecular chirality inversion, and (d) pH-induced chiroptical switching.

Similar achiral nanotubes have revealed capacity to specifically recognize chiral molecules resulting in a transition from racemic to homochiral helical nanotubes. In a very interesting example, a G-C motif equipped with achiral 4-aminobenzo-18-crown-6-ether was demonstrated to self-assemble into a racemic mixture of *P* and *M* helical nanotubes.²³ However, when chiral amino acid *L*-alanine was entrapped within the crown ether, the hierarchical organization of the corresponding supramolecular macrocycles led to the formation of helical nanotubes of a preferred handedness reflected by the emergence of CD activity.

The potential use of these systems has been undoubtedly demonstrated by the high number of publications related to applications in biomedical^{31–35} and environmental fields³⁶ among others.

Non-fused complementary nucleobases. Gonzalez-Rodriguez's research group described a novel molecular design involving rigid rod-like monomers with complementary nucleobases linked by linear, π -conjugated spacers. The formation of cyclic structures by this monomer structure was influenced by its

competition with the formation of linear oligomers as Watson-Crick edges could point to the same or opposite sides of the monomer. However, the molecular design provided a very strong chelate cooperativity to the system that favoured the formation of cyclic structures through Watson-Crick H-bonding interactions in a defined 90° geometry.^{37, 38} The symmetry of the H-bonding pattern also exerted a strong influence in the macrocyclization process. Thus, an asymmetric ADD-DAA H-bonding array led to more stable cycles than the symmetric DAD-ADA pattern, in which a higher number of degrees of freedom must be lost upon cyclotetramerization.³⁹ The effect of the number of σ -bonds in the *p*-oligoethynylbenzene spacer in the ability to form cycles was also evaluated. When this number was increased, the loss of rotational and torsional degrees of freedom upon cyclotetramerization increased and the chelate cooperativity therefore decreased. Then, the shorter the monomer, the stronger the chelate cooperativity and higher tendency to form cyclic structures.⁴⁰

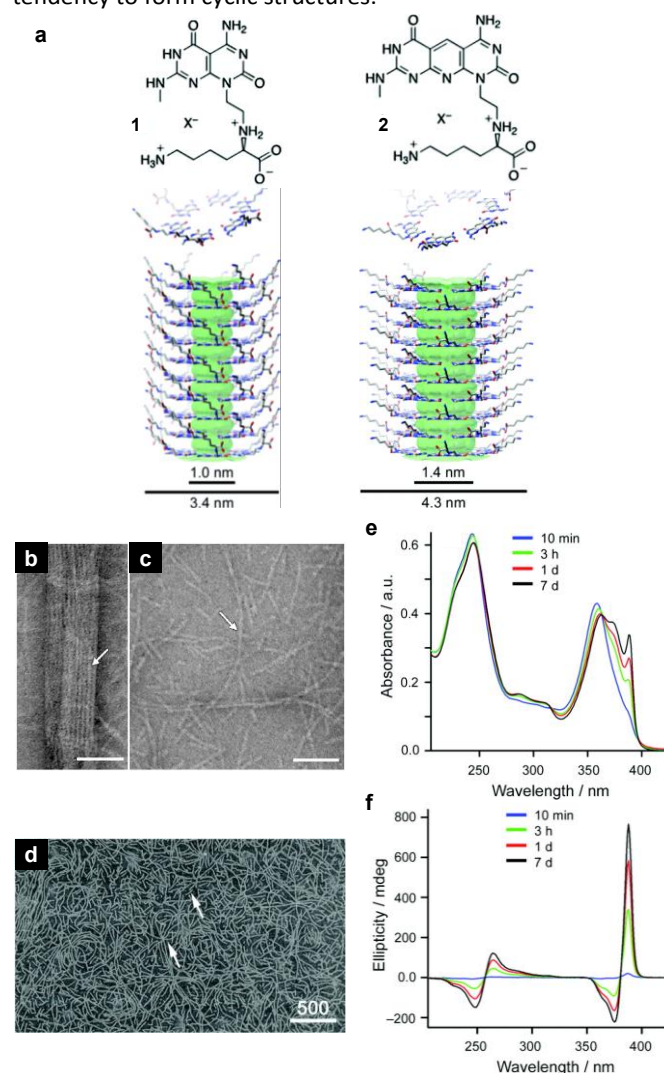


Fig. 2. (a) Chemical structure of compounds **1** and **2** and molecular model of the corresponding macrocycles and nanotubes formed. TEM images of the nanotubes obtained in water for (b) and (c) compound **1** and (d) compound **2**. (e) UV-Vis and (f) CD spectra of compound **2** (2×10^{-5} M in water). Adapted with permission from ref. 22 and 27. Copyrights 2001 and 2010, respectively, American Chemical Society.

The stacking of these cyclic tetramers into nanotubular structures was firstly investigated by Gonzalez-Rodriguez's research group in organic media.⁴¹ With this objective, molecule **3** was synthesized (Fig. 3). Long alkyl chains were attached to benzylic wedges at the nucleobases, guanine and cytosine, to enhance solubility in apolar solvents, and a peripheral amide group was also incorporated. In addition to this, lipophilic chiral chains were also included at the central block to promote a helical organization. With this design, polymerization could be produced through π - π interactions between planar cycles and H-bonds along the stacking axis (Fig. 3b). Both processes, macrocyclization and polymerization, were decoupled and could be investigated separately which allowed the control of the self-assembly process at both stages.

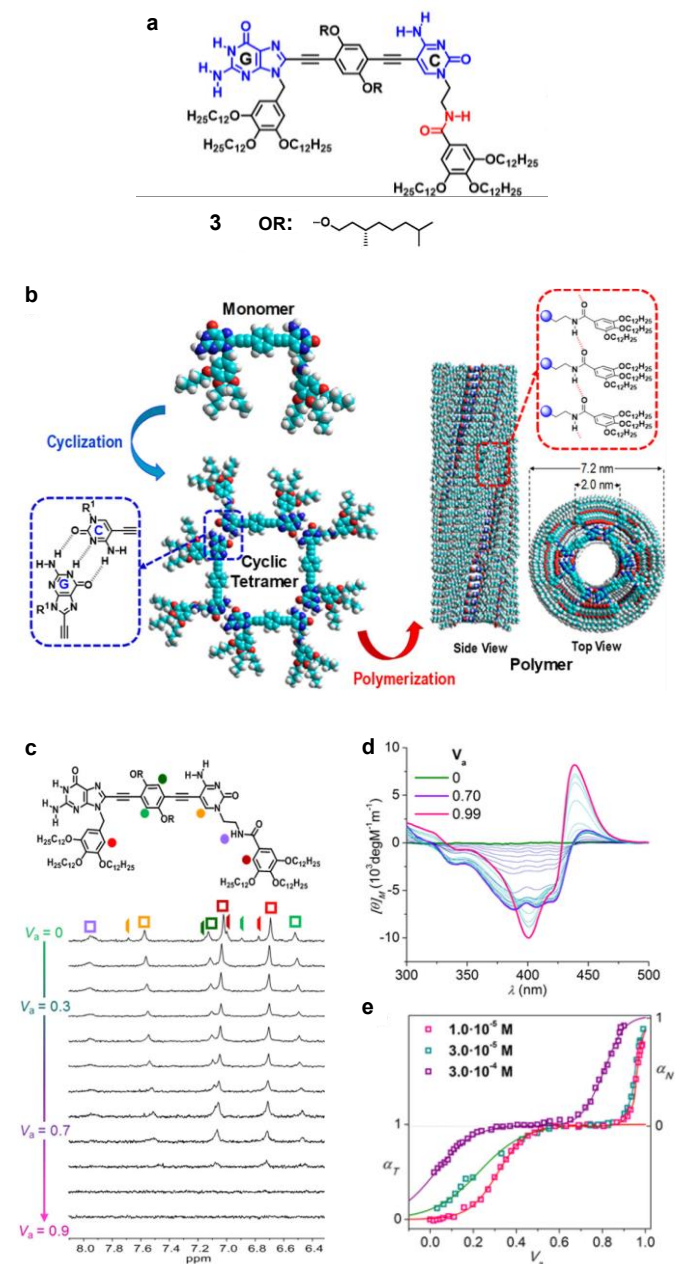


Fig. 3. (a) Chemical structure of compound **3**. (b) Schematic illustration of the self-assembly into cyclic tetramers and nanotubes. (c) T-dependent ¹H NMR experiments of compound **3** in the polymerization regime ($3 \cdot 10^{-4}$ M). (d) CD spectra of compound **3** as a function of the

volume fraction of heptane (V_a) in mixtures with THF ($3 \cdot 10^{-4}$ M). (e) Changes in the CD signal of compound **3** at 429 nm at several concentrations as a function of V_a (α_T = fraction of cyclotetramers, α_N = fraction of nanotubes). Adapted with permission from ref. 41. Copyright 2019, American Chemical Society.

When a solvent of intermediate polarity and intermediate H-bonding competing ability, like THF, was used, the equilibria from monomer to cyclic tetramer $c(\mathbf{3})_4$ could be followed. ¹H NMR spectra performed at low temperatures revealed a downfield shift of the G-amide and the C-amine proton signals, characteristic of the H-bonding between G and C in slow exchange with the corresponding monomer protons (Fig. 3c). The formation of the cyclic tetramer could be also monitored in THF by the red-shift in absorbance with a characteristic new maximum at 420 nm; a decrease in emission intensity and a marked red-shift; and the emergence of a CD Cotton effect, with the decrease of the temperature. When the volume fraction of heptane was increased in mixtures with THF up to 0.6, typical features of cyclotetramerization were observed. From 0.6 to 0.9 volume fraction, the cyclotetramer species was stabilized in solution and no spectroscopic changes were detected. However, at higher volume fraction, effects of an aggregation process were obtained: a broadening of tetramer protons and eventually disappearance; additional absorption red-shift, further quenching and slightly blue-shift of the emission; and a new Cotton effect (Fig. 3d). These changes were attributed to an aggregation process into chiral nanotubes driven by π - π stacking interactions between the large π -conjugated cycles and H-bonding interactions between the four peripheral amides. Monitoring the evolution of the CD features as a function of the heptane volume fraction, allowed to distinguish individually both self-assembly processes (Fig. 3e), and the data of the polymerization process could be fitted to a nucleation-elongation mechanism. The self-assembled nanotubes were characterized by DLS and small-angle X-ray scattering (SAXS), which proved the formation of large anisotropic aggregates of cylindrical organization with cylinder diameter of 4 ± 1 nm and a core diameter of about 1 nm. Moreover, SEM and TEM measurements confirmed the presence of networks of nanotube bundles with a measured diameter of 3.9 ± 0.7 nm, which coincides with the hard aromatic section of the cyclic tetramers.

A subsequent comparison study of this molecule with related ones in which the number of peripheral amides was varied from zero to two, allowed analysing the role of these functional groups in the two decoupled cooperative steps: cyclotetramerization and polymerization (Fig. 4).⁴² The analysis of the monomer-cyclotetramer equilibria revealed a markedly different stability of the macrocycles in THF: $c(\mathbf{5})_4 > c(\mathbf{4})_4 > c(\mathbf{3})_4$ caused mainly by slightly different association constants. The addition of heptane solvent into THF solution allowed the study of the second stage: the polymerization into chiral nanotubes. Two processes were observed for **3** and **5** (Fig. 4c and d) upon increasing the volume of heptane: the monomer-macrocycle equilibrium and the supramolecular polymerization of the tetramers. Whilst **3** exhibited a cooperative polymerization, **5** displayed an isodesmic polymerization. This difference could be

derived from the competition between intra- and intermolecular H-bonds and the different conformations of the pendant groups at the nucleobase C. On the other hand, and interestingly, **4** experienced only the cyclotetramerization process and was not able to polymerize (Fig. 4b and d). These findings indicated that the presence and number of peripheral amides plays indeed a key role in the formation of the polymeric nanotubes.

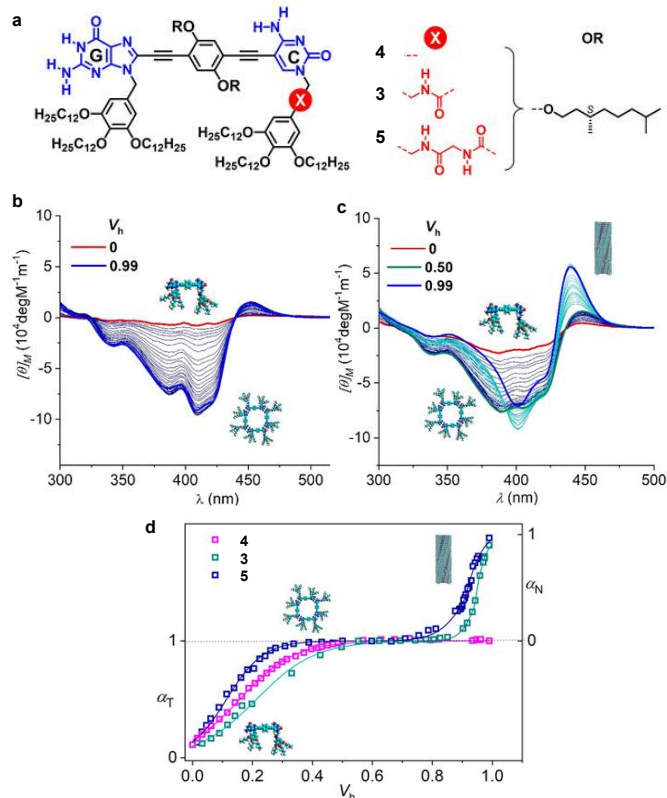


Fig. 4. (a) Chemical structure of compounds **3-5**. CD spectra of (b) compounds **4** and (c) **5** as a function of volume fraction of heptane (V_h) in mixtures with THF ($3 \cdot 10^{-5}$ M). (d) Normalized CD changes at 429 nm as a function of V_h for **3-5** (α_T = fraction of cyclotetramers, α_N = fraction of nanotubes). Adapted from ref. 42.

Following a similar strategy, a recent work published by Gonzalez-Rodriguez's research group was focused on building chiral nanotubes in aqueous environments.⁴³ For that purpose, some structural modifications were performed in the system. Amphiphilic alkyl chains were incorporated to molecule **6** to enhance its solubility in water and protect Watson-Crick pairing, and a hydrophilic ionic (carboxylate) group was attached to the *p*-phenylene block (Fig. 5). In that way, all the hydrophobic moieties were expected to be oriented to the inner part of the ensemble, exposing the hydrophilic chains to the aqueous environment (Fig. 5a). The spectroscopic features displayed by this compound in water were consistent with a chirally organized supramolecular structure. Moreover, the spectral changes found with temperature were fitted to a cooperative mechanism and were very similar to those described for the formation of nanotubes from macrocycles in organic media.⁴¹ ^1H NMR experiments at different $\text{H}_2\text{O}:\text{THF}-\text{D}_8$ compositions revealed ^1H signals for G:C pairing in slow exchange with

monomer signals. Moreover, the morphology and size of the nanotubes was studied by AFM (Fig. 5b) and TEM and the formation of tubular structures with width dimensions between 3 and 5 nm was confirmed. Finally, and in order to probe the ability of the nanotubes to extract and encapsulate apolar substances, the encapsulation of the well-known hydrophobic substance Nile Red (NR) was tested. Thus, the changes in spectral features of Nile Red alone in water and in the presence of nanotubes formed by **6** were analysed. When NR was mixed with **6**, an increase in its absorption and emission was observed, indicating that NR was solubilized by its encapsulation within the pore (Fig. 5c and d). Besides, the blue shift found for NR emission maximum (from 656 to 640 nm) was characteristic of this solvatochromic probe when surrounded by apolar environments. On the other hand, the intensity of the Cotton effect was reduced in the presence of NR because of the necessary rearrangement of chiral chains grouping within the pore when the guest is encapsulated in the tube (Fig. 5e). Finally, titration experiments in which increasing amounts of NR were added to a $1.0 \cdot 10^{-4}$ M water solution of **6** led to encapsulation efficiency values of around 0.2 equivalents of NR per molecule of **6**, that is, a maximum of about 5 molecules of compound **6** were able to host 1 NR molecule, which indicated that the dye was inserted in between cyclic tetramer sections.

The chiral organization of supramolecular systems can be influenced by the experimental conditions in which the monomers self-assemble. Very recently, an exploration about the self-assembly landscape in water of dinucleobase amphiphilic monomers equipped with hydrophilic groups at the π -conjugated central block of different nature: anionic (carboxylate), neutral (glycol) or cationic (ammonium) was reported (compounds **6**, **7** and **8** in Fig. 5, respectively).⁴⁴ The investigation of the aggregation was performed as a function of temperature, concentration and environment (which included solvent composition and pH). Even though, nanotube formation was reached for all compounds in varied experimental conditions, remarkable results were obtained when subtle changes in specific parameters or compound structure were applied. For instance, at high concentrations ($1.0 \cdot 10^{-4}$ M or higher) the CD signal of compound **6** did not disappear at high temperatures and changed in sign (Fig. 5g). This fact suggested that at these conditions compound **6** suffers a structural reorganization, as it was confirmed by TEM and AFM microscopy where nanotube bundles and ill-defined objects were observed presumably caused by dehydration of the polar groups. On the other hand, the change in the solvent composition also produced important changes in the self-assembly. Compounds **6** and **8** were insoluble in pure THF and their nanotube disassembly upon increasing the volume fraction of THF in water suggested the formation of other equilibrium intermediate aggregate(s). However, **7** showed aggregation in pure THF because of the presence of a CD signal (Fig. 5h) and an ill-defined ^1H NMR spectra. Moreover, only circular objects were observed in the corresponding AFM and TEM microscopy images. Finally, the pH also had a strong influence in the self-assembly of these compounds. Thus, compound **6** differed in its spectroscopic properties (CD, UV-vis

and emission) from acidic pH (pH = 3), compared to the ones observed at pH = 9 and pH = 5. At pH = 3 aggregate emission was quenched, CD spectra changed in shape and maxima (Fig.

5i) and absorbance decreased. Furthermore, when the acidic solution was heated at 85 °C at low concentration ($1.0 \cdot 10^{-5}$ M),

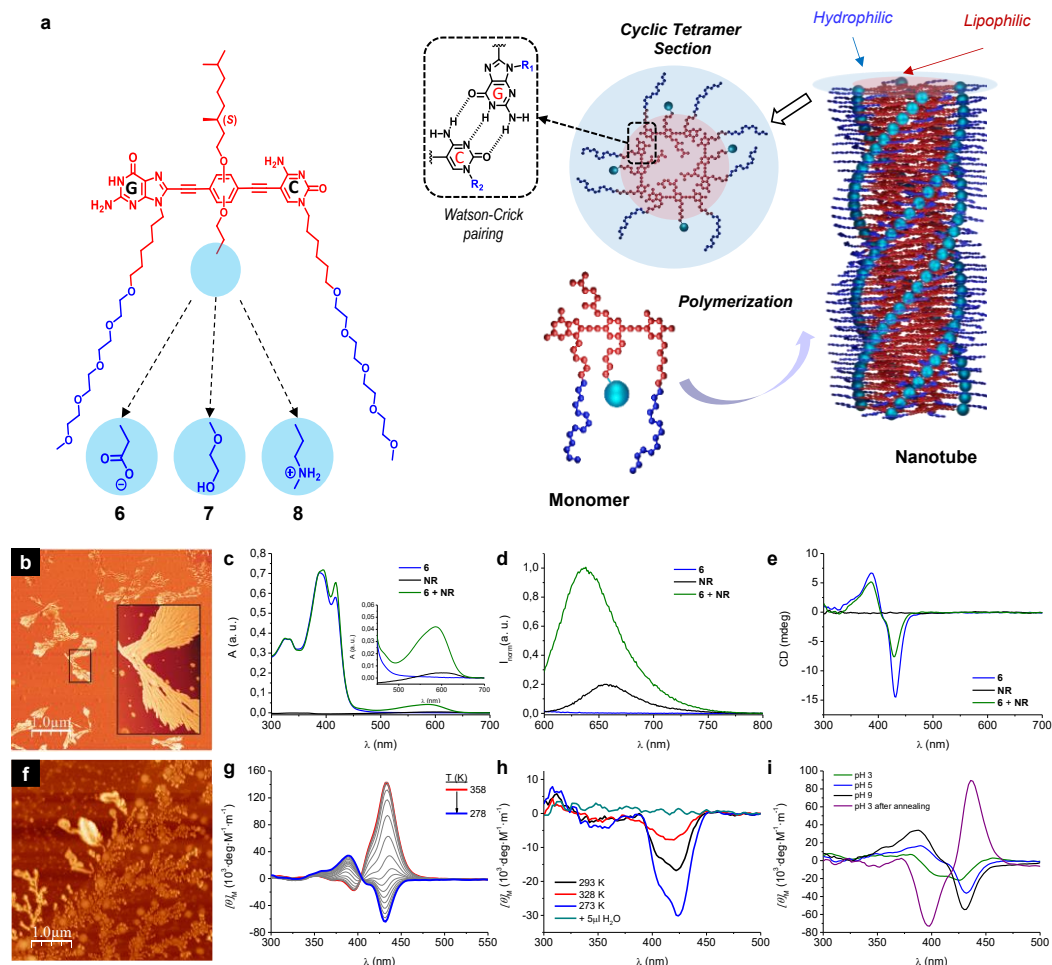


Fig. 5. (a) Structure of compound 6-8 and self-assembly into nanotubes. Hydrophobic and hydrophilic parts are represented in red and blue colours, respectively. (b) AFM images of the tubular structures formed by compound 6 in water. (c) Absorption, (d) emission and (e) CD spectra of compound 6 ($2 \cdot 10^{-4}$ M), NR ($2 \cdot 10^{-5}$ M) and a mixture of 6 ($2 \cdot 10^{-4}$ M) and NR ($2 \cdot 10^{-5}$ M) in water. (f) AFM image of the spherical objects formed by 6 at pH 3 ($1 \cdot 10^{-6}$ M). (g) Temperature-dependent CD spectra of 6 in H₂O at $1 \cdot 10^{-4}$ M. (h) CD spectra of 7 in THF at $1.0 \cdot 10^{-4}$ M at different temperatures and with the addition of H₂O. (i) Changes in the CD spectra of compound 6 as a function of the pH in water at $1 \cdot 10^{-5}$ M. Adapted from ref. 44 and with permission from ref. 43. Copyright, 2020, Wiley-VCH Verlag GmbH & Co. KGaA.

the inverse CD signal was detected, which was similar to the signal obtained for this compound at high temperatures and high concentrations, as previously mentioned. AFM and TEM images from this acidic solution showed again the presence of spherical objects (Fig. 5f). All these results suggested that drastic changes in the experimental conditions, can lead to chiral reorganization or a morphological restructuring into globular objects due to dehydration of the peripheral hydrophilic groups.

Non-natural nucleobases. Wärnmark's research group reported a new strategy for preparing supramolecular nanotubes making use of an enantiomerically pure bicyclo[3.3.1]nonane core fused with pyrrole and the non-natural nucleobase isocytosine with additional urea moieties appended to the isocytosine ring (compound 9 in Fig. 6).⁴⁵ This is an interesting example of the use of chiral synthetic cavities based on bicyclic rings to build supramolecular nanotubes. The incorporation of the electron-

rich pyrrole ring makes the 6[1H]-pyrimidinone form of the isocytosine unit the most stable tautomer where the terminal urea proton is H-bonded to an isocytosine nitrogen atom. In this way, the unit cannot adopt a self-complementary H-bonding array and several 2H-bonding sites positioned at different angles can be formed. However, the high level of preorganization can promote the cyclic aggregation of this compound. The formation of the corresponding cyclic structures in CHCl₃ was demonstrated by several NMR techniques like NOESY and diffusion-ordered spectroscopies, which led to a hydrodynamic radius, $R_H = 10$ Å, consistent with an aggregate significantly large, and in good agreement with tetrameric assemblies. When the polarity of the solvent was decreased to strengthen H-bonds in the system, the formation of larger aggregates was detected by the broadening of the ¹H NMR signals and the disappearance of the NH protons (Fig. 6b). The aggregation into large assemblies with chiral pores in

toluene was confirmed by AFM (Fig. 6c), DLS and GPC (*Gel Permeation Chromatography*) analyses. Interestingly, polymeric aggregates could also be formed in polar CDCl_3 solvent when a C_{70} guest was added. The use of Fourier transform infrared spectroscopy (FTIR) for a C_{70} :compound **9** mixture in CDCl_3 allowed probing the participation of the terminal urea moiety in the H-bonding for the tube propagation (Fig. 6d). In this experiment, the downshifts of the $\nu(\text{C}=\text{O})$ and the $\nu(\text{N}-\text{H})$ bands and the upshift of the $\nu_a(\text{C}-\text{N})$ band in the urea group were consistent with the involvement of urea in H-bonding interactions. This work constitutes the first example in which molecular tubes were assembled from organic molecules, where both the cycle formation and the polymerization were accomplished by H-bonding.

The change in the position and/or orientation of the H-bonding motif can determine the mode of aggregation. Thus, the replacement of isocytosine units in a related compound to the previous example by self-complementary 2-pyridinone H-bonding AD-DA motifs, favoured helical tubular oligomerization over cyclic aggregation.^{46, 47}

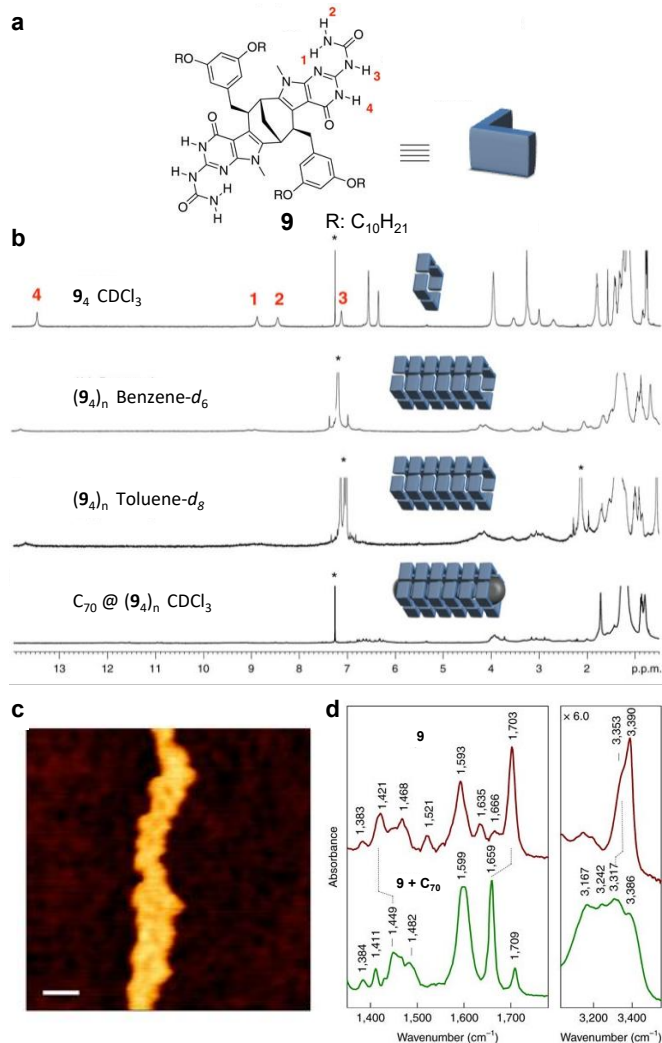


Fig. 6. (a) Chemical structure of compound **9**. (b) ^1H NMR spectra of **9** in different solvents and in the presence of C_{70} . (c) AFM image of the fiber-like superstructure formed by compound **9**. (d) FTIR spectra of **9** (top) and C_{70} /**9** 1:4 mixture (bottom) in CDCl_3 . Adapted from ref. 45.

However, isocytosine motifs can also act as self-complementary H-bonding units through tautomerization. In another work published by Wärnmark and col., two isocytosine rings non-equipped with urea groups were fused to a central enantiomerically pure bicyclo[3.3.1]nonane core (Fig. 7).⁴⁸ In that case, three DDA-AAD H-bonds between two different tautomeric isocytosine units led to the aggregation into cyclic tetramers that stacked on top of each other resulting in chiral tubular ensembles (Fig. 7b and d).

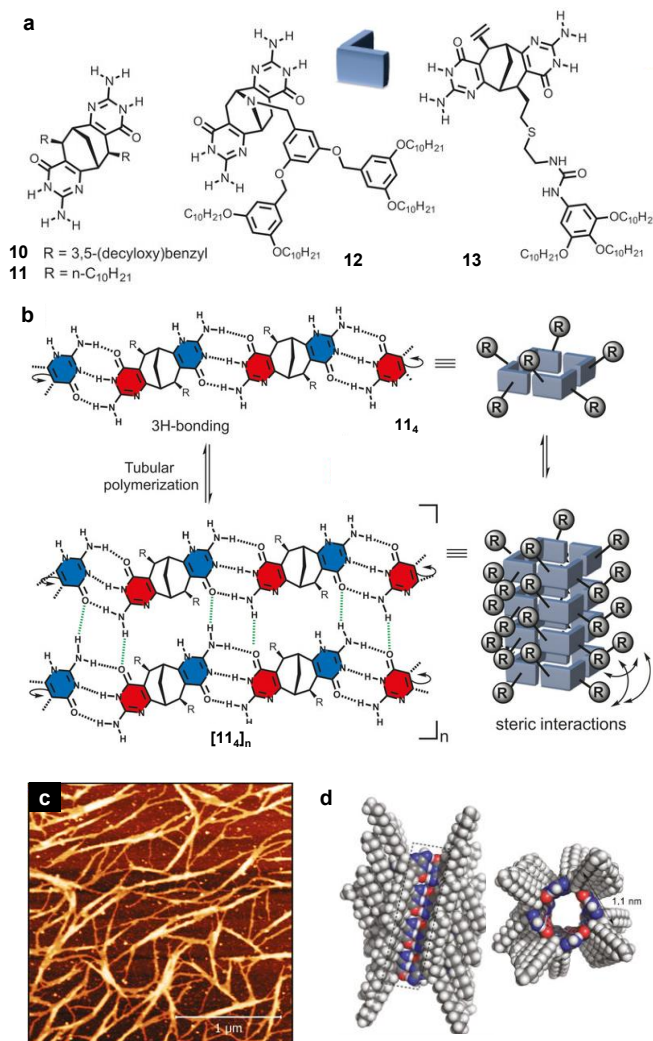


Fig. 7. (a) Chemical Structure of compounds **10-13**. (b) Schematic illustration of the two-directional aggregation into tubular structures. (c) AFM images of the fibrous network formed by **11** in CHCl_3 . (d) Molecular model of the tubular nanostructure obtained. Adapted from ref. 48.

With the objective of avoiding steric repulsion between bulky solubilizing groups in compound **10**, that can prevent the stacking of the cycles and the formation of the tubular ensemble, different size, position, or connectivity to the core were considered in new compounds **11**, **12** and **13**. The extremely broad and featureless ^1H NMR spectra and the high solution viscosity found for all new compounds in CHCl_3 and toluene, leading even to gels for compound **11** in both solvents, suggested the formation of polymeric aggregates. The tubular assemblies constituting the gel of compound **11** in toluene

could be filled by C₆₀ or C₇₀ guest molecules. However, racemic samples of compounds **11–13** were completely insoluble and didn't provide viscous solutions, gels or inclusion of C₆₀ or C₇₀ in a variety of solvents. This fact was indicative of the preferential heterochiral aggregation of monomers in racemates and the importance of using enantiomerically pure compounds for the construction of chiral H-bonded supramolecular tubular polymers. Moreover, high-resolution ¹H solid-state magic angle spinning (MAS) NMR spectroscopy performed on the dried gel of **11** demonstrated the tubular aggregation mechanism in which the two isocytosine tautomers were connected via 3 H-bonding. Finally, AFM images of a dried chloroform solution of **11** revealed a gel-like fibrous network structure composed of entangled bundles of tubular polymers (Fig. 7c).

Other approaches in which short tubes⁴⁹ or capsules⁵⁰ are obtained from related structures have been also reported by Wärnmark and Örenta's research group.

Oligophenylenes

Lee's group has extensively studied bent-shaped molecules formed by two segments of several benzene molecules joined together with a 120° of internal angle. Six-membered rings were formed in water by solvophobic interactions between monomers. These rings could stack on top of each other leading to supramolecular tubules with a hydrophobic pore and a hydrophilic outer core, provided with oligoether side-chains (Fig. 8a).⁵¹ When the self-assembly of compound **14** was investigated in aqueous solutions, nanotubes with an external diameter of 7 nm and a hollow interior diameter of 3 nm, were revealed by TEM microscopy (Fig. 8b). Absorption and emission experiments were carried out in water, which showed a quenched fluorescence intensity and a blue-shifted absorption maximum compared with those performed in chloroform, indicative of *H*-type stacking of the aromatic segments. Furthermore, CD spectroscopy exhibited a Cotton effect at concentrations of 0.002 wt %. All these observations suggested the aggregation of the molecules into nanotubes with a preferred helicity. In contrast, compound **15a**, equipped with a pyridine unit joining the two aromatic segments, was studied by DLS, TEM and AFM techniques and toroidal objects were displayed. An external diameter of 11 nm and 4 nm of inner cavity, as well as a height of 3.4 Å, were found, in accordance with a single six-membered macrocycle. Unlike compound **14**, the spectroscopic characteristics of compound **15a** in aqueous solutions exhibited a red-shifted absorbance maximum and an increase in the fluorescence intensity, indicative of *J*-type stacking of the aromatic segment. The expansion of the hexameric cycles could be explained by the formation of water clusters around the nitrogen at the pyridine unit, which would lead to a looser packing arrangement to reduce steric crowding at the valley position of the internal cavity. When concentration was increased, TEM images revealed the presence of elongated objects which conserved an external diameter of 11 nm and 4 nm of inner pore (inset in Fig. 8c). Also, the CD signal increased with the increase of the concentration (Fig. 8e top), corroborating the formation of nanotubes with a preferred

helicity. It should be pointed out that **15b**, the opposite enantiomer, displayed the inverse CD signal, indicating the transference of the molecular chirality to the supramolecular aggregates. The presence of ethylene oxide chains and pyridine units able to dehydrate upon heating, provided thermoresponsive behaviour to the system. When compounds **15a,b** were subjected to heating experiments, a contraction of the diameter of the nanotubes were observed by TEM (Fig. 8c and 8d bottom). Additionally, spectral changes like a blue-shifted absorption maximum and a quenching of the fluorescence intensity were recorded upon an increase of the temperature.

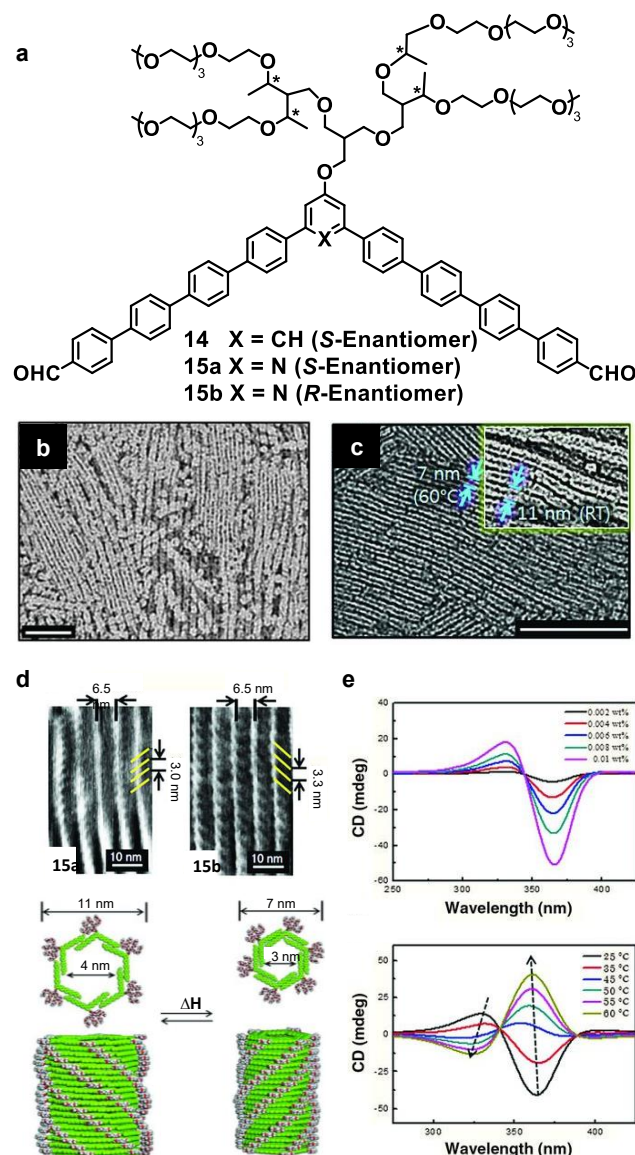


Fig. 8. (a) Chemical structure of compound **14** and **15a** and **15b**. TEM images of (b) **14** from 0.01 wt % aqueous solution and (c) **15a** from 0.01 wt % aqueous solution prepared at 60°C, (Inset) prepared at room temperature. (d) AFM phases images of the self-assembled right-handed (left) **15a** and left handed (right) **15b** nanotubes on HOPG and schematic representation of the reversible switching of the tubules of **15** upon heating. (e) Changes in the CD spectra of **15a** with the increase

of the (top) concentration and (bottom) temperature at 0.01 wt % in water. Adapted with permission from ref. 51. Copyright, 2012, American Association for the Advancement of Science.

All these spectroscopic changes were reversible in heating-cooling cycles. Remarkably, the primary CD signal displayed by compound **15a** dissolved in water, was inverted from a negative minimum into a positive Cotton effect upon heating (Fig. 8e bottom), indicating that the helical sense switched to the opposite handedness. This new positive signal resembled the temperature-independent CD signal of compound **14**, denoting that the new arrangement of compound **15a** at high temperatures adopted the same helicity. AFM images of **15a** and **15b** deposited on HOPG showed contracted tubules with opposite handedness (Fig. 8d), while expanded tubules of larger diameters were found when both solutions were deposited on hydrophilic mica substrates. Additionally, the encapsulation of hydrophobic guests like C₆₀ molecules into the inner cavity of the tubules formed by **15a** was demonstrated.

Making use of a derivative of compound **15a** with a shorter aromatic segment, Lee and co-workers could build nanofibers formed by dimers which subsequently were transformed into hollow nanotubes with a one-handed helical sense in the presence of a guest molecule.⁵² This inflation process involved the rearrangement of the compounds from dimers to hexameric macrocycles through reversible H-bonding interactions between the pyridine units of the aromatic cores and *p*-phenylphenol guest molecules. Remarkably, the weak Cotton effect observed for the aqueous solution of nanofibers increased considerably upon the addition of the guest, suggesting a more closed helical stacking of the aromatic segments in the presence of guest.

The morphological reorganization of tubular structures can be of use for different applications like in environmental sciences for the adsorption and release of pollutants. This is the case of the following example. The change in the self-assembly from porous tubules into solid fibers was obtained using a similar bent-shaped aromatic amphiphile to the one described in the previous example as a pH-sensitive segment.⁵³ In this system, the pH-sensitive central pyridine unit could be protonated, forming hexameric macrocycles, or deprotonated, forming dimeric disks. This rearrangement was accompanied by chiral inversion, the dimeric disks were stacked on top of each other forming right-handed solid fibers, whilst the hexameric cycles formed left-handed porous tubules. These nanotubes containing a switchable aromatic pore with superhydrophobicity could be used as nanopumps for the removal and controlled release of organic pollutants from water. The switching from right-handed solid fibers into left-handed tubules for efficient removal of pollutants was remarkably promoted by the (-)-acidic enantiomer of malic acid, whereas the contraction with full desorption of pollutants was incisively responsive to alkaline with (+)-conformation.

The co-assembly of this pH-sensitive segment with a rod-shape aromatic amphiphile could lead to the pH-driven formation of a dynamic 2D porous heterostructure through assembly-disassembly switching of the stacked macrocycles of

nanotubes and their subsequent spreading on the surfaces of a self-sorted sheet assembly in a hierarchical co-assembly.⁵⁴

Nanotubes based on oligophenylenes have been also used for catalytic purposes. In collaboration with Prof. Huang, Lee's research group synthesized bent-shaped compounds with a central pyridine and alkyl segments at both ends as hydrophobic units (Fig. 9a).⁵⁵ VPO measurements in ethanol of compounds **16** and **17** showed the formation of three membered macrocycles. The subsequent water addition into ethanol solutions promoted the stacking of the trimeric cycles on top of each other, leading to hollow tubules in both cases. TEM images displayed tubules for both compounds with an external diameter of 5.8 nm which were identical to those of trimeric macrocycles (Fig. 9b). Moreover, STEM (*Scanning Transmission Electron Microscopy*) experiments showed tubes with a hollow inner cavity of 2.3 nm. Both compounds displayed a blue-shifted absorption maximum and a quenched fluorescence intensity when water was added to an ethanol solution, indicating the formation of *H*-type aggregates. Besides, CD spectra of the nanotubes from compound **16** in ethanol/water solution showed a positive Cotton effect, indicative of the presence of nanotubes with a preferred helicity (Fig. 9c). In addition, AFM and X-ray techniques confirmed the formation of right-handed helical nanotubes with a helical pitch of 2.8 nm and an external diameter of 5.2 nm. On the contrary, molecule **17** did not display CD spectra, but nanotubes with 6 nm of diameter were observed by AFM. 2D XRD results suggested the formation of non-chiral nanotubes with larger interdistance between neighbouring cycles, due to the steric hindrance of the peripheral bulky alkyl groups (Fig. 9d). When a solution of achiral nanotubes of compound **17** was mixed with PdCl₂, the coordination of palladium ion to the pyridine unit was obtained. Taking advantage of the highly ordered porous structure and the stability of the Pd cation at the porous walls, the Pd-coordinated tubule of **17** could be used as a supramolecular catalyst with high activity for the Suzuki-Miyaura coupling with phenylboronic acid at ambient temperature.

Lee and co-workers also reported an interesting work studying the collective helicity switching of DNA embedded in a "synthetic coat" triggered by pH change.⁵⁶ The "synthetic coat" was formed by the mixed assembly of an achiral pyridine-bent-shape molecule, whose chiral derivative had already been reported previously,⁵⁷ and its pyridinium-based cationic derivative. Double-stranded DNA encapsulation in aqueous media was achieved by electrostatic interactions between pyridinium cations and the phosphate anions of DNA. At a pH value of 7.4 (physiological), right-handed native helicity of the encapsulated DNA was transferred to the coat assembly surrounding it. Lowering the pH to 5.5, helicity inversion occurred from right- to left-handed helical sense, and a contraction in the diameter of the coat assembly was noted, due to electrostatic interactions.

Lee's research group also published the self-assembly study of related compounds decorated with nitrile groups at both edges of the molecule to favour the hexameric macrocyclization

through complementary electrostatic interactions between electron-withdrawing nitrile groups and electron-donating

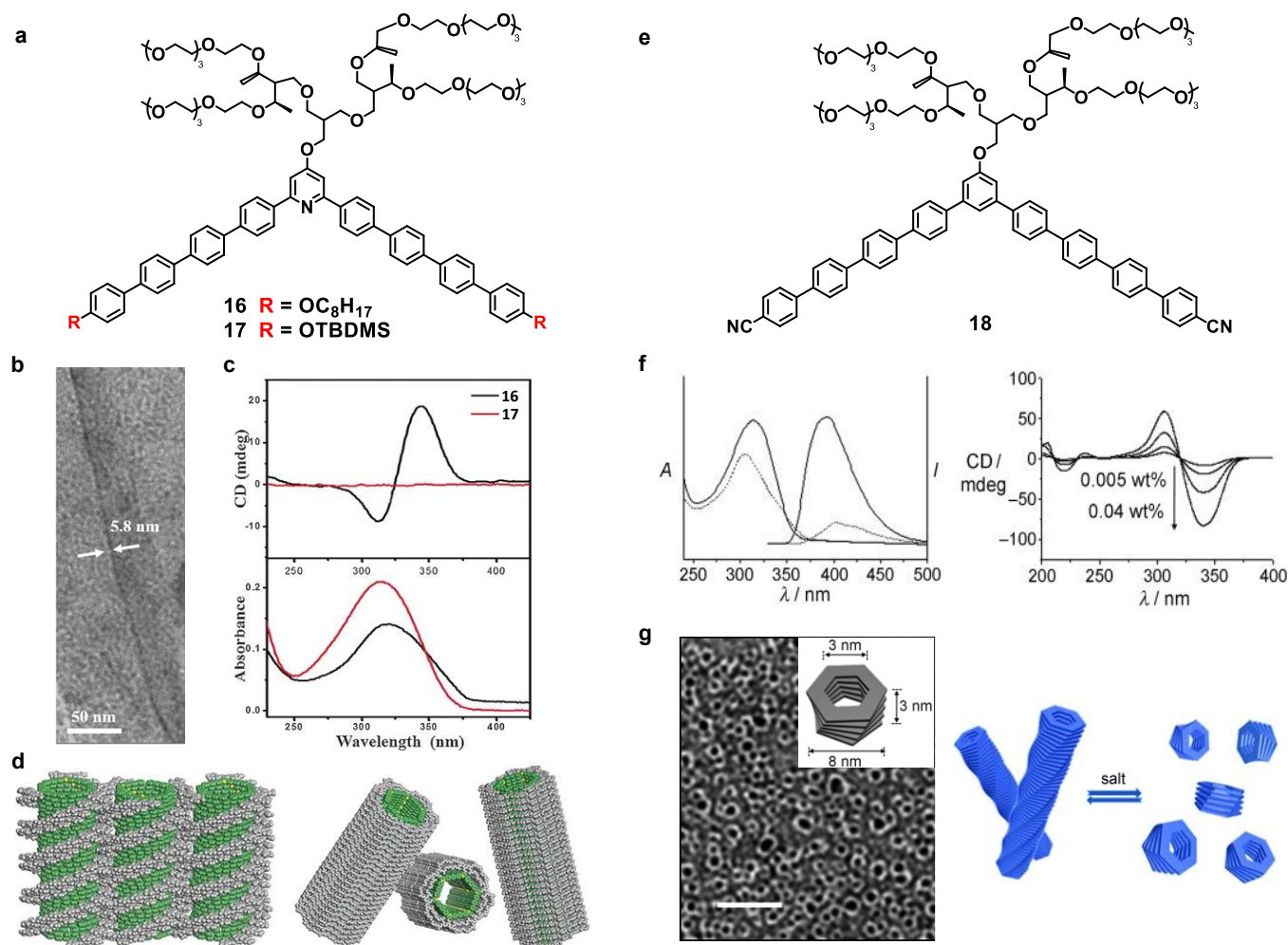


Fig. 9. (a) Structure of compounds **16** and **17**. (b) TEM image of **16** stained with uranyl acetate prepared from water/ethanol mixture. (c) Absorption and CD spectra of **16** and **17** in ethanol–water mixture (1:3, v/v, 0.01 wt%). (d) Representation of the helical aggregates formed by **16** (left) and alternative stacking of **17** (right). (e) Chemical structure of compound **18**. (f) (left) Absorption and emission spectra of compound **18** in $CHCl_3$ (solid line) and water (dashed line) at 0.02 wt %. (right) Concentration-dependent CD spectra of **18**. (g) TEM image of **18** with 10 equivalents of AgDS and schematic representation of the disassembly process. Adapted with permission from ref. 55 and 58. Copyrights, 2017 and 2010, respectively, Wiley-VCH Verlag GmbH&Co. KGaA.

phenoxy groups (compound **18** in Fig. 9e).⁵⁸ The red shift in the emission maximum and its decrease in intensity from aqueous solution to chloroform (Figure 9f left), as well as the emergence of a CD signal (Fig. 9f right), were ascribed to the aggregation into one-handed helical structures. Nanotube formation was confirmed by SAXS and TEM measurements, revealing nanotubes of 6 nm of external diameter with a hollow pore of 3 nm. The hydrophobic character of the pore and its functionalization with nitrile groups made that nanotube suitable for the encapsulation of hydrophobic silver salt through hydrophobic interactions together with silver–nitrile interactions in aqueous solution. The addition of up to 10 equivalents of silver dodecylsulfate (AgDS) produced a significant decrease of the hydrodynamic diameter from 65 nm to 8 nm, as confirmed by DLS. TEM and AFM measurements revealed the formation of toroidal objects consisting of helical stacks of several hexameric macrocycles by the dissociation of the nanotubes (Fig. 9g). Moreover, all the spectroscopic

properties were maintained with the addition of AgDS which demonstrated that the addition of guest molecules didn't influence the packing arrangement of the aromatic segments and the helical order of the tubular structure. These results provided a great example of controlling the dissociation of supramolecular structures upon addition of a metal-containing trigger.

Metal coordination complexes

Metals can also be used to construct macrocycles and to form tubular structures.^{59–65} An interesting example published also by Lee and co-workers describes a stimuli-responsive supramolecular structure able to be rearranged into metal-organic nanotubes with the addition of metal ions taking advantage of pyridine specific coordination to Ag (I) ions (Fig. 10).⁵⁹ Self-assembling molecule **19**, containing an aromatic segment equipped with *m*-pyridine units at both ends and

hydrophilic chiral chains, was proved to self-assemble in aqueous solution into flat sheets with a zigzag conformation of the aromatic segments by cryo-TEM. The red shift of the absorption maxima and the quenching of the fluorescence from chloroform to aqueous solution, were indicative of the presence of π - π interactions between aromatic segments. Even though molecule **19** contains chiral centers, no CD activity was observed for the system in water. Interestingly, upon addition of silver triflate, pyridine protons were downshifted in the NMR spectrum due to their interactions with metal ions and a CD signal emerged from this aqueous solution confirming the formation of chiral superstructures. The CD signal could be cancelled upon decomplexation by the addition of tetra-n-butylammonium fluoride (Bu_4NF) and restored again by addition of silver triflate (Fig. 10b) X.

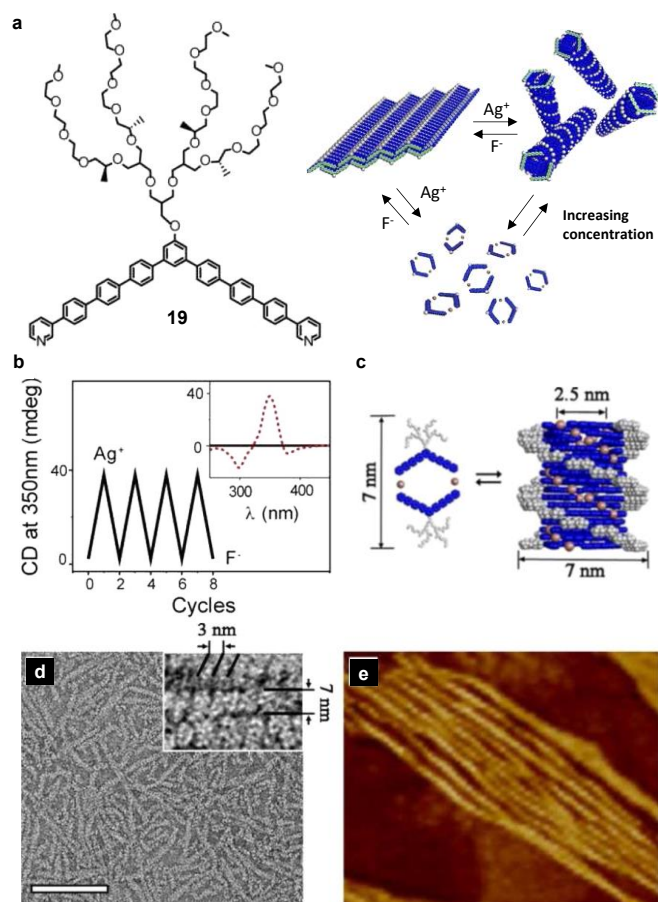


Fig. 10. (a) Chemical Structure of compound **19** and schematic illustration of the interconversion between flat sheets, helical tubules, and discrete toroids in response to external stimuli. (b) Reversible CD signal changes of an aqueous solution of **19** (0.03 wt %) upon cycles of complexation and subsequent decomplexation. The inset shows the CD spectra of the corresponding aqueous solution of **19** without Ag(I) ions (solid black line) and with Ag(I) ions (dotted red line). (c) Model of the dimeric macrocycle and tubular structure. (d) TEM and (e) AFM images of an aqueous solution of **19** with Ag(I) ions (0.03 wt %). Adapted with permission from ref. 59. Copyright, 2013, American Chemical Society.

This morphological transformation could be also followed by TEM. Images of casted aqueous solutions of molecule **19** and Ag(I) ions showed undulated helical objects with a uniform diameter of 7 nm and a left-handed helical sense with a pitch of

3 nm (Fig. 10c and d). The formation of helical objects was also confirmed by AFM (Fig. 10e). Additional DLS experiments using diluted solutions from 0.03 to 0.01 wt % revealed an abrupt decrease in the size from 200 to 8 nm, suggesting that the helical objects were originated from helical stacking of small objects rather than from helical folding of polymeric chains. Moreover, TEM and AFM measurements at 0.01 wt % showed toroidal structures, demonstrating that these objects were single stacks of macrocycles. These results corroborated the formation of dimeric macrocycles that stack on top of each other leading to tubular structures with a left-handed supramolecular chirality.

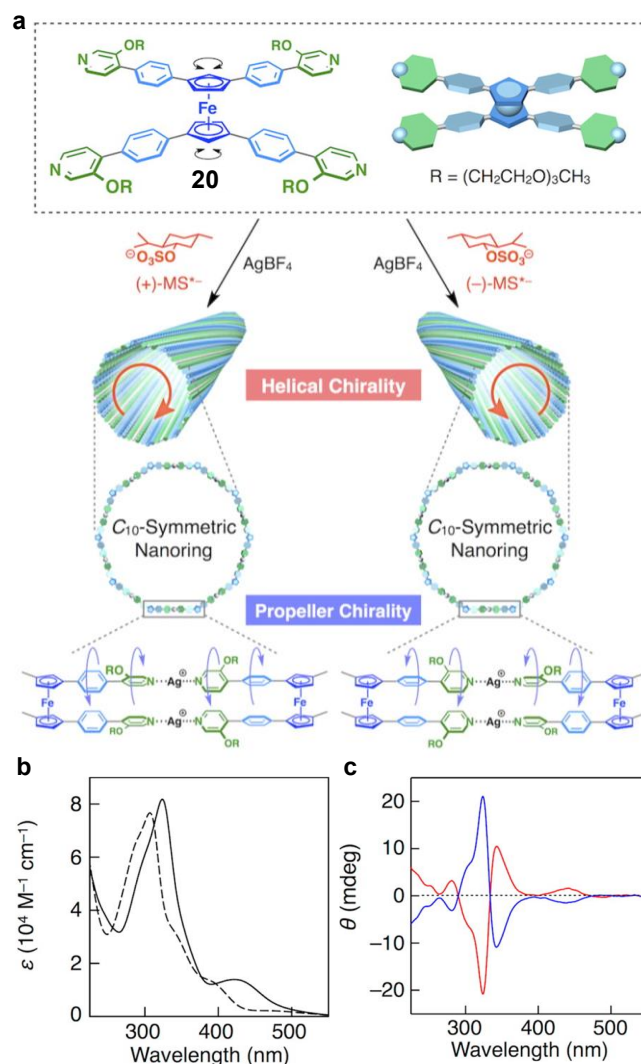


Fig. 11. (a) Chemical structure of compound **20** and schematic representation of its coassembly with AgBF_4 in the presence of (+)- or (-)-menthylsulfate (MS^*) into helical metal-organic nanotubes. (b) Absorption spectra of nanotubes (solid curve) prepared from **20** (100 μM), AgBF_4 (200 μM) and (-)- $\text{Bu}_4\text{N}^+\text{MS}^*$ (200 μM) and compound **20** alone (100 μM ; broken curve). (c) CD spectra of self-assembled nanotubes in presence of (+)- (red curve) and (-)- $\text{Bu}_4\text{N}^+\text{MS}^*$ (blue curve). Adapted with permission from ref. 61. Copyright, 2015, American Chemical Society.

Aida's research group reported an example of a co-assembly of ferrocene-cored tetratopic pyridyl ligand (**20**) and AgBF_4 in MeCN affording metal-organic nanotubes (Fig. 11).⁶⁰ In this

assembly, decagonal nanorings with large diameters of 7.5 nm, stacked on top of each other through π - π interactions and metallophilic (Ag-Ag) interactions. The XRD pattern obtained indicated that metal-organic nanotubes were composed of helical twists.⁶² When the co-assembly was performed in CH₂Cl₂/MeCN (7:3 v/v) in the presence of (+)- or (-)-menthylsulfate (MS*⁻), a red-shift of the absorption band from the non-assembled ligand was detected (Fig. 11b).⁶¹ TEM and AFM revealed tubular structures with a uniform diameter of 7.3 nm, and the proton signals of MS*⁻ disappeared due to bonding to Ag⁺. Moreover, mirror image CD signals were exhibited in the presence of (+)- and (-)-menthylsulfate (MS*⁻) and confirmed the formation of one-handed helical nanotubes (Fig. 11c).

Conclusions

In this feature article we have reviewed the most prominent examples of chiral nanotubes formed by the stacking of non-covalent macrocycles. Different chiral molecular structures have been used to date to build these hollow structures including nucleobases, oligophenylenes or metal coordination derivatives.

The success in the formation of cyclic structures depends mainly on the molecular design and consequently on the preorganization of the molecular structure. Thus, in the case of nucleobases, the H-bonding pattern and their location in the molecular structure are crucial factors to direct the non-covalent interactions in the correct orientation and position for ring closure. Solvophobic interactions are key forces for the macrocyclization of oligophenylene derivatives, whereas metals are also good candidates as they can form coordination bonds with specific chemical groups. In that sense, carefully designing a molecule with groups able to interact with metals in strategic positions is an interesting approach to obtain cyclic hollow structures.

Once the cycle has been formed, the involvement of secondary interactions, like π - π interactions and/or H-bonds, in the self-assembly process can easily promote the stacking of the cycles towards the desired nanotubes. These specific supramolecular nanotubes have been demonstrated to be stable both in apolar and polar, including water, solvents. Simply attaching chiral elements to the monomer unit it is possible to induce chirality from the molecular structure to the final assembly. Once again, the design in the molecular structure through the convenient attachment of chiral motifs results critical as it can be of use to specifically transfer chirality to the outer part of the nanotube, to the inner pore, or both.

We hope this feature article can serve as an inspiration for the future construction and study of novel chiral supramolecular nanotubes formed by the assembly of non-covalent cycles and for the translation of chiral properties into new supramolecular materials.

Acknowledgements

F. A. is grateful to MSCA-IF (793506) program. P. C. acknowledges the Comunidad de Madrid for the PEJ-2017-AI/IND-6246 contract. We also gratefully acknowledge Prof. D. Gonzalez-Rodriguez for his helpful comments.

Notes and references

- 1 J. Montenegro, M. R. Ghadiri and J. R. Granja, *Acc. Chem. Res.*, 2013, **46**, 2955-2965.
- 2 L. S. Shimizu, S. R. Salpage and A. A. Koros, *Acc. Chem. Res.*, 2014, **47**, 2116-2127.
- 3 W. Si, P. Xin, Z.-T. Li and J.-L. Hou, *Acc. Chem. Res.*, 2015, **48**, 1612-1619.
- 4 T. Shimizu, W. Ding and N. Kameta, *Chem. Rev.*, 2020, **120**, 2347-2407.
- 5 R. L. Beingessner, Y. Fan and H. Fenniri, *RSC Advances*, 2016, **6**, 75820-75838.
- 6 E. Yashima, N. Ousaka, D. Taura, K. Shimomura, T. Ikai and K. Maeda, *Chem. Rev.*, 2016, **116**, 13752-13990.
- 7 B. Adhikari, X. Lin, M. Yamauchi, H. Ouchi, K. Aratsu and S. Yagai, *Chem. Commun.*, 2017, **53**, 9663-9683.
- 8 A. Nitti, A. Pacini and D. Pasini, *Nanomaterials*, 2017, **7**, 167.
- 9 T. Shimizu, *Bull. Chem. Soc. Jpn.*, 2018, **91**, 623-668.
- 10 A. R. A. Palmans and E. W. Meijer, *Angew. Chem. Int. Ed.*, 2007, **46**, 8948-8968.
- 11 Y. Dorca, E. E. Greciano, J. S. Valera, R. Gómez and L. Sánchez, *Chem. Eur. J.*, 2019, **25**, 5848-5864.
- 12 K. Ariga, T. Mori, T. Kitao and T. Uemura, *Adv. Mater.*, 2020, **32**, 1905657.
- 13 X.-X. Cheng, T.-F. Miao, L. Yin, W. Zhang and X.-L. Zhu, *Chin. J. Polym. Sci.*, 2021.
- 14 C. A. Hunter and H. L. Anderson, *Angew. Chem. Int. Ed.*, 2009, **48**, 7488-7499.
- 15 F. Aparicio, M. J. Mayoral, C. Montoro-García and D. González-Rodríguez, *Chem. Commun.*, 2019, **55**, 7277-7299.
- 16 D. Serrano-Molina, A. de Juan and D. González-Rodríguez, *Chem. Rec.*, 2021, **21**, 480-497.
- 17 P. Ballester and J. d. Mendoza, in *Modern Supramolecular Chemistry*, eds. F. Diederich, P. J. P. J. Stang and R. R. Tykwinski, Wiley-VCH 2008, pp. 69-111.
- 18 S. Di Stefano and G. Ercolani, in *Adv. Phys. Org. Chem.*, eds. I. H. Williams and N. H. Williams, Academic Press, 2016, vol. 50, pp. 1-76.
- 19 P. Motloch and C. A. Hunter, in *Adv. Phys. Org. Chem.*, eds. I. H. Williams and N. H. Williams, Academic Press, 2016, vol. 50, pp. 77-118.
- 20 D. T. Bong, T. D. Clark, J. R. Granja and M. R. Ghadiri, *Angew. Chem. Int. Ed.*, 2001, **40**, 988-1011.
- 21 J.-L. Hou, in *Hydrogen Bonded Supramolecular Structures*, eds. Z.-T. Li and L.-Z. Wu, Springer Berlin Heidelberg, Berlin, Heidelberg, 2015, pp. 249-267.
- 22 H. Fenniri, P. Mathivanan, K. L. Vidale, D. M. Sherman, K. Hallenga, K. V. Wood and J. G. Stowell, *J. Am. Chem. Soc.*, 2001, **123**, 3854-3855.
- 23 H. Fenniri, B.-L. Deng and A. E. Ribbe, *J. Am. Chem. Soc.*, 2002, **124**, 11064-11072.
- 24 J. G. Moralez, J. Raez, T. Yamazaki, R. K. Motkuri, A. Kovalenko and H. Fenniri, *J. Am. Chem. Soc.*, 2005, **127**, 8307-8309.
- 25 R. S. Johnson, T. Yamazaki, A. Kovalenko and H. Fenniri, *J. Am. Chem. Soc.*, 2007, **129**, 5735-5743.
- 26 G. Borzsonyi, A. Alsbaiee, R. L. Beingessner and H. Fenniri, *J. Org. Chem.*, 2010, **75**, 7233-7239.
- 27 G. Borzsonyi, R. L. Beingessner, T. Yamazaki, J.-Y. Cho, A. J. Myles, M. Malac, R. Egerton, M. Kawasaki, K. Ishizuka, A. Kovalenko and H. Fenniri, *J. Am. Chem. Soc.*, 2010, **132**, 15136-15139.

- 28 T. Yamazaki, H. Fenniri and A. Kovalenko, *ChemPhysChem*, 2010, **11**, 361-367.
- 29 A. Marsh, M. Silvestri and J.-M. Lehn, *Chem. Commun.*, 1996, 1527-1528.
- 30 U. D. Hemraz, M. El-Bakkari, T. Yamazaki, J.-Y. Cho, R. L. Beingessner and H. Fenniri, *Nanoscale*, 2014, **6**, 9421-9427.
- 31 J. D. Ede, V. A. Ortega, D. Boyle, R. L. Beingessner, U. D. Hemraz, H. Fenniri, J. L. Stafford and G. G. Goss, *Toxicol. Sci.*, 2015, **148**, 108-120.
- 32 M. L. Puzan, B. Legesse, R. A. Koppes, H. Fenniri and A. N. Koppes, *ACS Biomater. Sci. Eng.*, 2018, **4**, 1630-1640.
- 33 J.-Y. Cho, P. Bhowmik, P. L. Polowick, S. G. Dodard, M. El-Bakkari, G. Nowak, H. Fenniri and U. D. Hemraz, *ACS Omega*, 2020, **5**, 24422-24433.
- 34 X. Zhou, S. Tenaglio, T. Esworthy, S. Y. Hann, H. Cui, T. J. Webster, H. Fenniri and L. G. Zhang, *ACS Appl. Mater. Interfaces*, 2020, **12**, 33219-33228.
- 35 P. Tripathi, L. Shuai, H. Joshi, H. Yamazaki, W. H. Fowle, A. Aksimentiev, H. Fenniri and M. Wanunu, *J. Am. Chem. Soc.*, 2020, **142**, 1680-1685.
- 36 J. D. Ede, V. A. Ortega, D. Boyle, R. L. Beingessner, U. D. Hemraz, H. Fenniri, J. L. Stafford and G. G. Goss, *Environ. Sci.: Nano*, 2016, **3**, 578-592.
- 37 C. Montoro-García, J. Camacho-García, A. M. López-Pérez, N. Bilbao, S. Romero-Pérez, M. J. Mayoral and D. González-Rodríguez, *Angew. Chem. Int. Ed.*, 2015, **54**, 6780-6784.
- 38 J. Camacho-García, C. Montoro-García, A. M. López-Pérez, N. Bilbao, S. Romero-Pérez and D. González-Rodríguez, *Org. Biomol. Chem.*, 2015, **13**, 4506-4513.
- 39 C. Montoro-García, J. Camacho-García, A. M. López-Pérez, M. J. Mayoral, N. Bilbao and D. González-Rodríguez, *Angew. Chem. Int. Ed.*, 2016, **55**, 223-227.
- 40 C. Montoro-García, M. J. Mayoral, R. Chamorro and D. González-Rodríguez, *Angew. Chem. Int. Ed.*, 2017, **56**, 15649-15653.
- 41 V. Vázquez-González, M. J. Mayoral, R. Chamorro, M. M. R. M. Hendrix, I. K. Voets and D. González-Rodríguez, *J. Am. Chem. Soc.*, 2019, **141**, 16432-16438.
- 42 V. Vázquez-González, M. J. Mayoral, F. Aparicio, P. Martínez-Arjona and D. González-Rodríguez, *ChemPlusChem*, 2021, **86**, 1087-1096.
- 43 F. Aparicio, P. B. Chamorro, R. Chamorro, S. Casado and D. González-Rodríguez, *Angew. Chem. Int. Ed.*, 2020, **59**, 17091-17096.
- 44 P. B. Chamorro, F. Aparicio, R. Chamorro, N. Bilbao, S. Casado and D. González-Rodríguez, *Org. Chem. Front.*, 2021, **8**, 686-696.
- 45 Q. Shi, T. Javorskis, K.-E. Bergquist, A. Ulčinas, G. Niaura, I. Matulaitienė, E. Orentas and K. Wärnmark, *Nat. Comm.*, 2017, **8**, 14943.
- 46 S. Stončius, E. Orentas, E. Butkus, L. Öhrström, O. F. Wendt and K. Wärnmark, *J. Am. Chem. Soc.*, 2006, **128**, 8272-8285.
- 47 E. Orentas, C. J. Wallentin, K. E. Bergquist, M. Lund, E. Butkus and K. Wärnmark, *Angew. Chem. Int. Ed.*, 2011, **50**, 2071-2074.
- 48 A. Neniškis, D. Račkauskaitė, Q. Shi, A. J. Robertson, A. Marsh, A. Ulčinas, R. Valiokas, S. P. Brown, K. Wärnmark and E. Orentas, *Chem. Eur. J.*, 2018, **24**, 14028-14033.
- 49 D. Rackauskaite, R. Gegevicus, Y. Matsuo, K. Wärnmark and E. Orentas, *Angew. Chem. Int. Ed.*, 2016, **55**, 208-212.
- 50 D. Račkauskaitė, K.-E. Bergquist, Q. Shi, A. Sundin, E. Butkus, K. Wärnmark and E. Orentas, *J. Am. Chem. Soc.*, 2015, **137**, 10536-10546.
- 51 Z. Huang, S.-K. Kang, M. Banno, T. Yamaguchi, D. Lee, C. Seok, E. Yashima and M. Lee, *Science*, 2012, **337**, 1521-1526.
- 52 Y. Wang, Z. Huang, Y. Kim, Y. He and M. Lee, *J. Am. Chem. Soc.*, 2014, **136**, 16152-16155.
- 53 S. Bao, S. Wu, L. Huang, X. Xu, R. Xu, Y. Li, Y. Liang, M. Yang, D. K. Yoon, M. Lee and Z. Huang, *ACS Appl. Mater. Interfaces*, 2019, **11**, 31220-31226.
- 54 X. Liu, H. Li, Y. Kim and M. Lee, *Chem. Commun.*, 2018, **54**, 3102-3105.
- 55 S. Wu, Y. Li, S. Xie, C. Ma, J. Lim, J. Zhao, D. S. Kim, M. Yang, D. K. Yoon, M. Lee, S. O. Kim and Z. Huang, *Angew. Chem. Int. Ed.*, 2017, **56**, 11511-11514.
- 56 Y. Kim, H. Li, Y. He, X. Chen, X. Ma and M. Lee, *Nat. Nanotechnol.*, 2017, **12**, 551-556.
- 57 H.-J. Kim, F. Liu, J.-H. Ryu, S.-K. Kang, X. Zeng, G. Ungar, J.-K. Lee, W.-C. Zin and M. Lee, *J. Am. Chem. Soc.*, 2012, **134**, 13871-13880.
- 58 H.-J. Kim, S.-K. Kang, Y.-K. Lee, C. Seok, J.-K. Lee, W.-C. Zin and M. Lee, *Angew. Chem. Int. Ed.*, 2010, **49**, 8471-8475.
- 59 S. Shin, S. Lim, Y. Kim, T. Kim, T.-L. Choi and M. Lee, *J. Am. Chem. Soc.*, 2013, **135**, 2156-2159.
- 60 T. Fukino, H. Joo, Y. Hisada, M. Obana, H. Yamagishi, T. Hikima, M. Takata, N. Fujita and T. Aida, *Science*, 2014, **344**, 499-504.
- 61 H. Yamagishi, T. Fukino, D. Hashizume, T. Mori, Y. Inoue, T. Hikima, M. Takata and T. Aida, *J. Am. Chem. Soc.*, 2015, **137**, 7628-7631.
- 62 M. Obana, T. Fukino, T. Hikima and T. Aida, *J. Am. Chem. Soc.*, 2016, **138**, 9246-9250.
- 63 P. D. Frischmann, S. Guieu, R. Tabeshi and M. J. MacLachlan, *J. Am. Chem. Soc.*, 2010, **132**, 7668-7675.
- 64 P. D. Frischmann, B. J. Sahli, S. Guieu, B. O. Patrick and M. J. MacLachlan, *Chem. Eur. J.*, 2012, **18**, 13712-13721.
- 65 Z. Chen, B. J. Sahli and M. J. MacLachlan, *Inorg. Chem.*, 2017, **56**, 5383-5391.